



University of Latvia

FACULTY OF PHYSICS, MATHEMATICS AND  
OPTOMETRY

**Katrīna Laganovska**

**DEFECTS AND OPTICAL PROPERTIES  
OF UNDOPED AND RARE-EARTH  
DOPED  $\text{HfO}_2/\text{ZrO}_2$**

SUMMARY OF DOCTORAL THESIS

Submitted for the Degree of Doctor of Physics  
Subfield of Material Physics

Scientific supervisor: PhD. Phys. Krišjānis Šmits

RĪGA, 2023

The doctoral thesis was carried out at University of Latvia, Faculty of Physics and Mathematics, Institute of Solid State Physics from 10.2017. until 05.2023.

Form of thesis: dissertation in Physics, Subfield of Material Physics.

Scientific supervisor:

**Dr. Phys. Krišjānis Šmits**, leading researcher, head of Laboratory of Microscopy, Institute of Solid State Physics, University of Latvia.

Reviewers:

- 1.
- 2.
- 3.

The thesis will be defended at the public session of the Doctoral Committee of Physics and Astronomy, University of Latvia at xxx on xxx in the Conference hall of the Institute of Solid State Physics of University of Latvia.

The thesis will be available at the Library of the University of Latvia, Kalpaka blvd 4., Riga, Latvia.

Chairman of Doctoral Committee  
Ferbbers

Dr. habil. phys. Ruvins

Secretary of Doctoral Committee

Sintija Siliņa

© Katrīna Laganovska, 2023

© University of Latvia, 2023

## Abstract

Hafnium oxide currently replaces silicon dioxide as the gate oxide in metal-oxide-semiconductor transistors of ultra-high density integrated circuits. It is selected due to its high dielectric constant, broad band gap, chemical stability, and compatibility with silica. Furthermore, the discovery of a ferroelectric phase existence in hafnia has opened up its use in applications such as ferroelectric random-access memories, ferroelectric transistors and others.

The main challenge presented by hafnia is its relatively high amount of intrinsic defects. Defects lead to larger leakage currents in thin films, reduce the chemical stability, impact the stability of the ferroelectric phases and overall affect the characteristics and properties of the material.

This work, therefore, focuses on the **study of intrinsic defects found in hafnia and its twin oxide zirconia**, using luminescent probes to gather information about defect surroundings and origins, as well as using thermoluminescence to determine the exact type of defects present and their excitation energies. Despite numerous theoretical studies on the subject, a thorough experimental investigation had not yet been performed.

The main topics covered in this thesis are:

1. Impact of the vicinity and distribution of oxygen vacancies on the resulting rare-earth ion luminescence.
2. Use of rare-earth ion probes as a way to monitor the sintering processes in ceramics.
3. Identification of oxygen vacancy types in monoclinic hafnia.
4. Rare-earth ion incorporation characteristics in monoclinic hafnia.

Hafnia is a highly promising electronic material and the knowledge of causes, types, and characteristics of intrinsic defects present provides a new understanding of how to limit these defects and improve the overall properties to further advance the quality of the material and its uses in high-demand applications.

# CONTENTS

<b>1</b>	<b>Introduction</b>	<b>7</b>
1.1	Motivation . . . . .	7
1.2	Aim . . . . .	8
<b>2</b>	<b>Literature review</b>	<b>9</b>
2.1	Intrinsic defects . . . . .	9
2.1.1	Theoretical studies . . . . .	9
2.1.2	Experimental studies . . . . .	10
2.2	Photoluminescence . . . . .	11
2.3	Thermoluminescence . . . . .	12
<b>3</b>	<b>Methods</b>	<b>13</b>
<b>4</b>	<b>Results and discussion</b>	<b>15</b>
4.1	Charge compensation in hafnia . . . . .	15
4.1.1	Introduction . . . . .	15
4.1.2	Results and discussion . . . . .	15
4.1.3	Conclusions . . . . .	20
4.1.4	Thesis 1 . . . . .	20
4.2	Formation of translucent nanostructured zirconia ceramics . . . . .	22
4.2.1	Introduction . . . . .	22
4.2.2	Results and discussion . . . . .	22
4.2.3	Conclusions . . . . .	28
4.2.4	Thesis 2 . . . . .	29
4.3	Thermoluminescence study of oxygen vacancies in HfO <sub>2</sub> . . . . .	30
4.3.1	Introduction . . . . .	30

4.3.2	Results and discussion . . . . .	31
4.3.3	Conclusions . . . . .	35
4.3.4	Thesis 3 . . . . .	35
4.4	Europium ion incorporation characteristics in HfO <sub>2</sub> . . . . .	36
4.4.1	Introduction . . . . .	36
4.4.2	Results and discussion . . . . .	36
4.4.3	Conclusions . . . . .	40
4.4.4	Thesis 4: . . . . .	40
<b>5</b>	<b>Summary</b>	<b>42</b>
<b>6</b>	<b>Theses</b>	<b>44</b>
<b>7</b>	<b>List of conferences and publications</b>	<b>45</b>
7.1	Authors publications reflecting the thesis . . . . .	45
7.2	Other publications . . . . .	47
7.3	Conferences . . . . .	49
<b>8</b>	<b>Acknowledgements</b>	<b>50</b>
<b>9</b>	<b>References</b>	<b>51</b>

# 1. INTRODUCTION

## 1.1 Motivation

Following Moore's law (the number of transistors in an integrated circuit doubles about every two years) (Moore, 1975), the scaling down of silicon dioxide dielectrics was formerly thought to be a useful way to improve transistor performance in complementary metal-oxide semiconductor (CMOS) technology. Reduced silicon dioxide gate dielectric thickness has permitted larger numbers of transistors per chip with improved circuit functionality and performance at cheap costs in recent decades.

However, as devices approach the sub-45 nm scale, the effective oxide thickness of typical silicon dioxide dielectrics must be less than 1 nm, which is around 3 monolayers and close to the physical limit, resulting in large gate leakage currents due to the obvious quantum tunneling effect. To keep the downward scaling going, dielectrics with a higher dielectric constant (high-k) are being proposed as a way to get the same transistor performance while keeping the physical thickness low (Chau et al., 2004).

Because of its desirable features such as a broad band gap of 5.25–5.95 eV (Jiang et al., 2010) and a high-k value of 25 (Huang A.P., 2010), hafnia has become a popular choice among high dielectric constant materials for CMOS. Hafnia also has a higher heat of formation than silica and has excellent chemical compatibility with silicon, as well as being chemically and thermally stable. Because gate stacks go through quick thermal annealing processes, this is very critical for the silica contact. Additionally, the recent discovery of a ferroelectric phase existence and the aforementioned properties, make hafnia a promising material for ferroelectric field-effect transistor (FeFET) and ferroelectric random-access memory (FeRAM) applications (Böscke et al., 2011). Compared to  $\text{SiO}_2$ ,  $\text{HfO}_2$  has a higher defect concentration, resulting in a higher density of charge traps, transient

instability of the gate threshold voltage, Coulomb scattering of carriers in the substrate channel, and source-level voltage instability. Therefore it is of great importance to study the defects in  $\text{HfO}_2$  and its twin oxide  $\text{ZrO}_2$ , which is the focus of this study.

## 1.2 Aim

The aim of this work is to study the defects and optical properties in undoped and doped  $\text{HfO}_2$  and  $\text{ZrO}_2$  in order to understand the influence of defects such as oxygen vacancies on the resulting characteristics of these materials.

Four hypotheses were formed and the following theses were confirmed:

**Thesis 1:** The luminescence intensity of rare-earth ions in  $\text{HfO}_2$  is determined more by the vicinity and distribution of nearby oxygen vacancies than by phase transition from monoclinic to tetragonal.

**Thesis 2:** Erbium ion luminescence is an effective way of monitoring defect formation and phase transformation in nanostructured  $\text{ZrO}_2$  ceramics during the sintering process.

**Thesis 3:** Single (+1) and double (+2) charged oxygen vacancies at 3-fold coordinated ( $\text{VO}_3^{1+}$ ,  $\text{VO}_3^{2+}$ ) and 4-fold coordinated ( $\text{VO}_4^{1+}$  +  $\text{VO}_4^{2+}$ ) sites of monoclinic  $\text{HfO}_2$  can be identified by thermoluminescence.

**Thesis 4:** In monoclinic  $\text{HfO}_2$ ,  $\text{Eu}^{3+}$  ions tend to incorporate in pairs as well as single ions, creating  $\text{VO}_3^{2+}$  and  $\text{VO}_3^{1+}$  oxygen vacancies.

## 2.LITERATURE REVIEW

### 2.1 Intrinsic defects

While  $\text{HfO}_2$  and  $\text{ZrO}_2$  are used in this study interchangeably, this section will focus more on  $\text{HfO}_2$  as that is the material represented in Thesis 3 and 4, where the following information is applied more in detail than for Thesis 1 and 2.

#### 2.1.1 Theoretical studies

Like most materials, hafnia can contain defects that can significantly affect its performance. Intrinsic defects in hafnia, such as oxygen vacancies and hafnium interstitials, have been a topic of discussion for many years due to their impact on the electrical, optical, and mechanical properties of the material.

The work of Foster (Foster et al., 2002) shows that interstitial oxygen species and charged vacancies may serve as traps for electrons from the hafnia conduction band. Oxygen vacancies also exhibited "negative-U" behavior, i.e.,  $\text{VO}^{1+}$  was not stable against disproportionation into  $\text{VO}^0$  and  $\text{VO}^{2+}$ , although their behavior could not be predicted with any precision due to the underestimated band gap.

The calculations of Xiong et al. place the vacancy levels much higher than Foster (Foster et al., 2002) and are more consistent with charge trapping data, indicating that the oxygen vacancy is the most common defect in  $\text{HfO}_2$  gate oxide films.

The work of Zheng confirms oxygen interstitials have a "negative-U" characteristic that is consistent with studies by Foster et al. Because an oxygen interstitial adds three 2p states and four 2p electrons to the top of the valence band, the defect levels caused by oxygen interstitials had

valence-band characteristics, and the formation energy for oxygen interstitials was unlikely to be significantly influenced by the band gap underestimation in the work of Foster.

Additionally, Chimata further shows that under oxygen-poor conditions, the positively charged oxygen defects  $\text{VO}^{1+}$  and  $\text{VO}^{2+}$  have negative formation energies, indicating that they will form spontaneously.

### 2.1.2 Experimental studies

Kiisk (Kiisk et al., 2010) proposes the excitation band at 4.2 eV being related to charge transfer transitions from the valence band to singly or doubly ionized oxygen vacancies. A similar case is also found in yttrium stabilized zirconia (YSZ), where the recombination of a hole in the valence band with an electron trapped at the oxygen vacancy promotes the vacancy into an excited state, resulting in a 2.4 eV emission (Petrik et al., 1999).

Gritsenko (Gritsenko et al., 2016) shows that the thermal activation energy for the thermoluminescence peak near 372 K is 1.25 eV, as measured in the charge transport studies. It is concluded, that the peak around 372 K is caused by an oxygen vacancy. Gritsenko further suggests that the thermoluminescence peaks at temperatures 255, 291, and 315 K are caused by oxygen polyvacancies in  $\text{HfO}_2$  based on similarities with other studies (Kaichev et al., 2013; Perevalov et al., 2013).

Shilov et al. (Shilov et al., 2022) notes that according to calculations (Gavartin et al., 2006; Muñoz Ramo, Gavartin, et al., 2007), oxygen vacancies in different charge states of  $\text{O}_3$  and  $\text{O}_4$  create new energy levels in the forbidden gap, with corresponding optical transitions defining spectral characteristics of the optical absorption spectrum. The sharp increase in absorption at  $h\nu > 5.5$  eV corresponds to the typical monoclinic hafnia intrinsic absorption edge and also coincides with the excitation energy of the STE (self-trapped excitons) (Aarik et al., 2004; Franta et al., 2011; Manikantan et al., 2017). Heavy holes are then thought to cluster at the

top of the valence band at  $2p$  orbitals of  $O_3$  atoms (Muñoz Ramo, Shluger, et al., 2007). Furthermore, similar to other transition metal oxides, more mobile electrons can be captured to states near the bottom of the conduction band (CB), which are dominated by the narrow  $5d$  orbitals of hafnium atoms (Muñoz Ramo, Shluger, et al., 2007). As a result these characteristics indicate that excitons in monoclinic  $HfO_2$  with 4.2 eV luminescence have a self-trapping nature (Gritsenko et al., 2016; Kirm et al., 2005; Kong et al., 2019; Villa et al., 2018).

## 2.2 Photoluminescence

In this study, the applications of europium and erbium luminescent probes are employed. Luminescent probes that consist of rare-earth materials offer a way to obtain a more comprehensive understanding of the symmetry and local structures of the host materials. Moreover, they enable us to make inferences about the origin of oxygen vacancies in hafnia.

The photoluminescence spectra of undoped  $HfO_2$  and  $ZrO_2$  is usually characterised by a broad PL band, centered at around 2.5 eV, consisting of several subbands. The origin of PL in undoped metal oxides is often explained by the intrinsic defects present in the host material.

While the literature does not provide a thorough analysis of the potential origins of these subbands, the most intense band (2.5 eV) has been identified as an  $F^+$  center - an anion vacancy with a missing electron. This band has been identified due to its very fast ns decay time is similar to the decay time values of  $F^+$  centers in several oxides (Aleksanyan et al., 2016; Rosenblatt et al., 1989; Villa et al., 2016).

For an isolated europium ion, all  $4f^6$  intraconfigurational transitions are forbidden electrical dipole transitions. When an europium ion is embedded in a matrix it interacts with the local crystal field. The mixing of states of different parities caused by the local symmetry distortion eventually leads to partially allowed electric dipole transitions. Magnetic dipole transitions are allowed by spin-orbit coupling between various states, re-

sulting in independence on local symmetry in the first order. This means that the degree of distortion of the  $\text{Eu}^{3+}$  site in relation to the centrosymmetric configuration can be determined by comparing the intensities associated with electric dipole and magnetic dipole transitions (Binnemans and Görrler-Walrand, 1996).

For erbium, the green emission is observed from the  ${}^4\text{S}_{3/2} \rightarrow {}^4\text{I}_{15/2}$  transition while the  ${}^4\text{F}_{9/2} \rightarrow {}^4\text{I}_{15/2}$  transition produces red emission. The increase in overall emission intensity in the presence of  $\text{Yb}^{3+}$  ions and  $\text{Er}^{3+}$  ions is consistent with the idea that the energy transfer process between these ions is dependent on their concentration and location. This suggests that the efficiency of the transfer process increases as the concentration of  $\text{Yb}^{3+}$  and  $\text{Er}^{3+}$  ions increases and the resulting correlation of red to green luminescence offers valuable insights into the host material (Patra et al., 2002).

## 2.3 Thermoluminescence

Thermoluminescence in this work is used to determine the types of oxygen vacancies present in hafnia and their activation energies.

Thermoluminescence is the thermally stimulated emission of light following the previous absorption of energy from radiation (McKeever, 1983).

To determine trap depth levels in this work, the following second-order deconvolution function developed by Chen et al. (1970)(Chen and Winer, 1970) is used

$$I_m = n_0 s \exp\left(-\frac{E}{kT_m}\right) \left[ \frac{skT_m^2}{\beta E} \exp\left(-\frac{E}{kT_m}\right) (1 - \Delta_m) + 1 \right]^{-2} \quad (2.1)$$

where  $\Delta_m = 2kT_m/E$ ,  $I_m$  is the glow peak intensity,  $E$  (eV) the activation energy,  $s$  ( $\text{s}^{-1}$ ) the frequency factor,  $n_0$  the initial concentration of trapped carriers,  $k$  ( $\text{eV K}^{-1}$ ) the Boltzmann constant,  $T_m$  (K) the absolute temperature of the peaks,  $\beta$  (K/min) the heating rate.

### 3.METHODS

X-ray diffraction (XRD) was measured using PANalytical X'Pert Pro diffractometer with Cu K $\alpha$  radiation (1.5418 Å). The morphology of all samples was characterized by high-resolution SEM- FIB electron microscope Helios 5 UX (Thermo Scientific) operated at 2 kV using the TLD (through-the-lens detector) detector.

For lamella preparation samples were covered with gold. The crystalline size verification and morphology studies were performed using a transmission electron microscope (TEM, Tecnai G20, FEI) operated at 200 kV. The samples for TEM studies were placed on a holey carbon coated grid AGS147-4 (Agar Scientific).

Two different setups were utilized for luminescence measurements. The first setup included an Andor Shamrock SR-303i spectrometer paired with an Andor iDus401 CCD for the measurement of photoluminescence spectra, TL studies, and XRL. The second setup was a Horiba iHR320 imaging spectrometer combined with a SampleMax sample chamber and a Jobin Yvon/Horiba TRIAX320 excitation monochromator, which was used for the measurement of photoluminescence and luminescence decay kinetics. This spectrometer was also coupled with a photomultiplier tube and CCD.

In addition to Andor Shamrock SR-303i and Andor iDus401 setup, TL measurements were performed by **Lexsyg Research TL/OSL reader** from Freiberg Instruments with samples being irradiated by X-rays for 30min before measuring TL.

The decay kinetics of luminescence were measured using a photon counting head **H8259-02 (HAMAMATSU)** and a **P7887 counting board** (Fast Com Tec GmbH) with minimal time bin 0.25 ns. The time resolution of the system was 1 ns.

The majority of the software used was for graphical data representation, performing deconvolution functions on the obtained data and analysing X-

ray diffractograms. Non-specific software used is not mentioned.

**OriginPro** is a scientific data analysis and graphing software. It provides tools for data analysis, graphing, and programming, and was used for creating graphical representations in this work. Additional scripts using the built-in programming language LabTalk were created for more efficient use of the software.

**Mathematica** provides a wide range of functions for numerical and symbolic computations, visualization, and programming. A custom script was used for deconvolution calculations for both photoluminescence and thermoluminescence spectra.

**Profex** software was used for the analysis of X-ray diffractograms and the determination of the phases of the materials using Rietveld refinement.

# 4.RESULTS AND DISCUSSION

## 4.1 Charge compensation in hafnia

### Hypothesis 1:

A hypothesis is put forward that the distribution and concentration of oxygen vacancies determine the resulting rare-earth ion luminescence intensity rather than the surrounding crystal symmetry and phase. This is explored by doping hafnia with a charge-compensating element such as  $\text{Nb}^{5+}$  in addition to the  $\text{Eu}^{3+}$  ions. When a charge-compensating element is introduced, the amount of oxygen vacancies is reduced and as a result, the phase of the host material remains monoclinic and is not transformed to tetragonal. This allows us to judge the intensity of luminescence in different conditions.

### 4.1.1 Introduction

Recent studies (Puust et al., 2017; Robertson et al., 2006; Smits et al., 2014) showed that in zirconia a strong overall reduction in lanthanide ( $\text{Ln}^{3+}$ ) luminescence intensity can be explained by intrinsic defects. However, the implementation of  $\text{Nb}^{5+}$  ions as charge compensators in the matrix can change the defect concentration and distribution thus highly increasing the resulting intensity. Zirconia and hafnia have very similar optical, electrical and structural properties, therefore, they are called twin oxides. Hence in this study, we are looking at Nb effect on Eu ion luminescence in hafnia.

### 4.1.2 Results and discussion

The aim of this research was to study the role of Nb ions in the crystalline structure, and  $\text{Nb}^{5+}$  ion concentration was chosen to match the lanthanide

concentration, similar to previous studies (Kiisk et al., 2017; Smits et al., 2017). This decision was based on the fact that for each pair of ions only one oxygen vacancy is needed to compensate the charge. No vacancies are needed to form monoclinic phase, which means that  $\text{Ln}^{3+}$  ions are non-uniformly distributed in the matrix and tend to agglomerate (especially at higher temperatures monoclinic phase and large grain size). Samples with less than 5 mol% content did not seem to provide any additional information and were not studied. A lower luminescence intensity and monoclinic phase would be expected as is seen in similar studies in  $\text{ZrO}_2$  (Tamrakar et al., 2015) and (Meng et al., 2010).

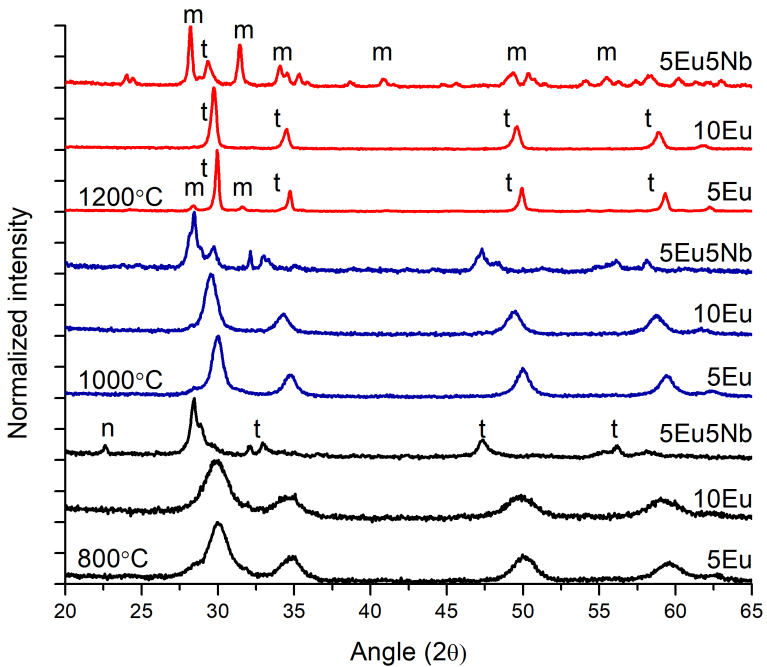


Figure 4.1: Hafnia structure dependence for all annealing temperatures and dopant concentrations (XRD)

As it is expected for the structure and the resulting luminescence in-

tensity of hafnia to be dependent on the size of nanocrystal grains, all samples were annealed at three different temperatures: 800°C , 1000°C , 1200°C , similar to the approach used in other research works (Meng et al., 2010; Smits et al., 2014; Smits et al., 2017).

X-ray diffraction (XRD) data (Fig.4.1) revealed that when the annealing temperature was increased to 1200°C , phase transformation from tetragonal to monoclinic started taking place in the sample 5Eu (5mol% Eu). This phase transformation is assumed to happen due to nanocrystal grain size increase which results in excess surface energy being insufficient for stabilization (Smits et al., 2017). For the sample containing Nb, the monoclinic phase was dominant for all annealing temperatures and at lower temperatures, besides the presence of monoclinic and tetragonal phases, additional phases of Nb<sub>2</sub>O<sub>5</sub> can be seen. This means that the chosen method of synthesis does not ensure the creation of pure hafnia phases only, although niobium related phases disappear with the increase of the annealing temperature. Previous research demonstrates that inability to remain stable in a tetragonal phase for samples containing Nb is due to the resulting oxygen vacancy decrease in the crystallites (Smits et al., 2014). Ln<sup>3+</sup> ions are expected to not take part in tetragonal phase stabilizations due to oxygen vacancies not forming as a result of the charge compensation. Crystallite sizes were calculated using the Scherrer equation (Langford and Wilson, 1978) and were found to be (in nm): 5.8, 10.6, 48.4 for 5Eu samples, 5.3, 9.4, 26.5 for 10Eu and 13.4, 16.4, 45.5 for 5Eu5Nb for annealing temperatures of 800°C , 1000°C , 1200°C , respectively.

Sample 10Eu (10mol% Eu) maintained a steady tetragonal phase for all annealing temperatures due to the relatively large Ln<sup>3+</sup> concentration. It can be seen that the stabilization of tetragonal phases is dependent on Eu ion concentration and 5mol% is not sufficient for higher (>1000°C ) annealing temperatures. However the concentration of 5mol% in various metal oxides is considered to be optimal for maximum luminescence intensity and phase stabilization (Meng et al., 2010; Smits et al., 2014).

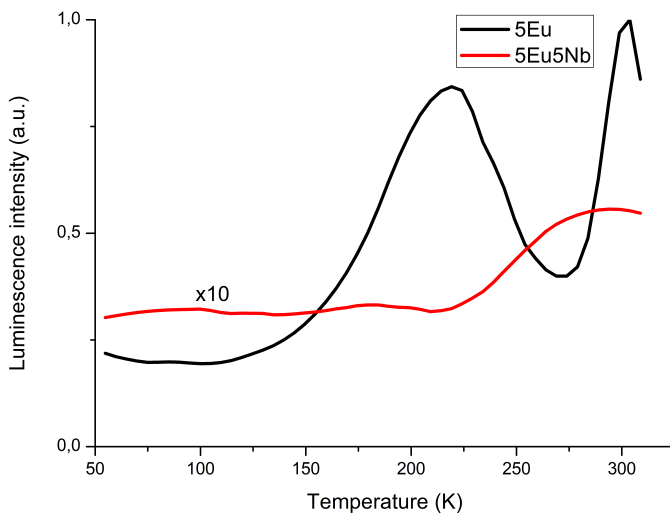


Figure 4.2: TL intensity distribution for peaks at 613nm.

The oxygen vacancies in the  $\text{HfO}_2$  matrix act as electron traps and as such, they have their characteristic TL (Fig.4.2) curves. Therefore, to determine the relative number of defects in samples with and without Nb, thermoluminescence measurements were performed for samples 5Eu and 5Eu5Nb (5mol%Eu and 5mol%Nb), annealed at  $1200^\circ\text{C}$ . The spectra show Eu ion luminescence. TL peaks for the  ${}^5\text{D}_0 \rightarrow {}^7\text{F}_2$  transition were monitored over all temperatures. Luminescence intensity throughout heating was ten times greater for the sample 5Eu, confirming a significant decrease in defects (electron traps) for the sample containing Nb, of which most are assumed to be oxygen vacancies (Hu et al., 2009).

For samples annealed at  $800^\circ\text{C}$ , the most intense luminescence was observed for the sample containing 5% Eu (Fig.4.3). With the increase of annealing temperatures, oxygen vacancies are thought to relocate between  $\text{Ln}^{3+}$  ions wherever charge compensation is needed. The distance to the oxygen vacancies becomes smaller as the temperature rises, thus increasing the chances for the photons coming from  $\text{Ln}^{3+}$  ions to get trapped in the

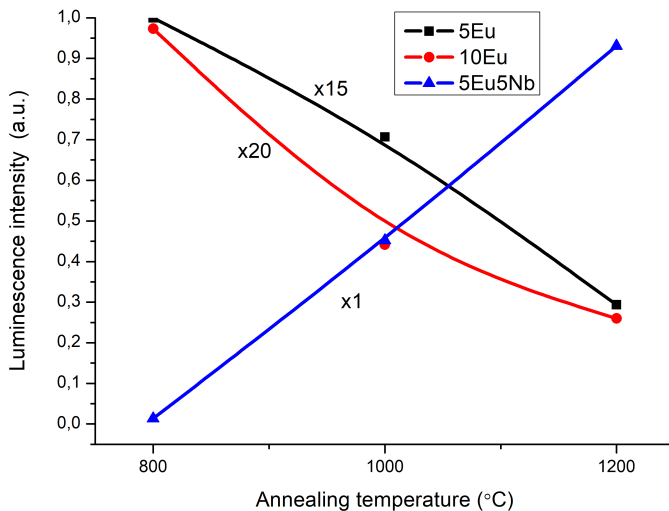


Figure 4.3: Integrated photoluminescence intensity (570-670nm range) dependence on annealing temperatures.

defects.

Luminescence intensity for the Nb doped sample increases by a great margin for samples annealed at higher temperatures. We associate the lesser luminescence intensity seen at lower annealing temperatures with Eu ion mixing with  $\text{Nb}_2\text{O}_5$  phases, as the tenfold increase in luminescence for higher temperatures could not be explained solely by larger particle sizes or a decrease in defects.

At 1000°C and 1200°C the most intense luminescence was observed for the sample containing Nb, excluding the possibility that the increase in intensity of the Nb doped samples is a positive effect of  $\text{Nb}_2\text{O}_5$  presence. Despite the larger grain sizes, with the increase in annealing temperature from 800°C to 1200°C the luminescence intensity halves for samples without Nb. This counterintuitive behaviour can be explained with the cation inability to diffuse at temperatures below 1200°C, therefore an anion diffusion takes place in the oxygen sublattice. The luminescence quenching is

explained with oxygen vacancies present in the near vicinity of Eu ion (in the first coordination sphere). Similar behaviour has been shown in other research works (Liu et al., 2010).

### 4.1.3 Conclusions

This study demonstrates that the Nb ions implemented in 4th group oxides doped with lanthanide ions drastically increase the luminescence intensity.  $\text{HfO}_2$  is the second metal-oxide system where this effect is demonstrated, therefore other similar systems are expected to fall in this category too. Doping with 5% Eu is not sufficient for phase stabilization at higher temperatures, however samples doped with 10% Eu show lower luminescence intensity due to concentration quenching. Sample containing Nb has a significantly higher luminescence intensity starting at 1000°C and higher. The partial phase change from mostly tetragonal to mostly monoclinic accompanied by an increase in luminescence intensity in the samples containing Nb, indicates that the changes in luminescence intensity for samples not containing Nb are mostly due to oxygen vacancy presence and are not directly related to changes in the phase of crystallites and the resulting local crystal field. The calculated quantum efficiency also indicates a fivefold increase for the sample containing Nb annealed at 1200°C.

### 4.1.4 Thesis 1

The thesis of this study is therefore that the vicinity and distribution of oxygen vacancies determine the resulting rare-earth ion luminescence in  $\text{HfO}_2$  rather than the surrounding crystal symmetry and phase. As it was seen, while the phase change from tetragonal to monoclinic in purely europium-doped samples seems to result in a reduction in the luminescence intensity, when the material is additionally doped with the charge-compensating element niobium, the phase change does not affect the re-

sulting luminescence intensity and it increases with increasing annealing temperatures.

**Thesis 1:** The luminescence intensity of rare-earth ions in  $\text{HfO}_2$  is determined more by the vicinity and distribution of nearby oxygen vacancies than by phase transition from monoclinic to tetragonal.

## 4.2 Formation of translucent nanostructured zirconia ceramics

### Hypothesis 2:

A hypothesis is put forward that erbium ion luminescence is an effective way of monitoring defect formation and phase transformation in nanostructured  $\text{ZrO}_2$  ceramics during the sintering process. In order to prove this hypothesis, zirconia samples are formed using the sol-gel method and solar physical vapor deposition and are doped with erbium. The pressure applied when pressing the powder into pellets impacts the phase of the resulting ceramics - this is thus monitored by studying rare-earth up-conversion luminescence in the different samples as the surroundings of the crystal change.

### 4.2.1 Introduction

Zirconium dioxide ( $\text{ZrO}_2$ ) is a good potential material for use in nano/structured ceramics (Yamashita et al., 2012) as it has a wide band gap and a relatively large refraction coefficient (Smits et al., 2013; Yamashita et al., 2012) compared to similar materials. The goal of this thesis is to study the formation of translucent nanostructured ceramics. Research of mechanisms that affect the optical translucency was carried out by doping the translucent  $\text{ZrO}_2$  ceramics with  $\text{Er}^{3+}$ ,  $\text{Yb}^{3+}$  and performing XRD, up-conversion luminescence, TEM and SEM studies.

### 4.2.2 Results and discussion

To understand the origin of the color of the ceramic and to study ceramic sintering, after pressing the nanoparticle powder into ceramic pellets (250 MPa, diameter of pellet 5 mm, thickness 1 mm) the samples underwent annealing in air at various temperatures – 500°C, 700°C, 800°C and 900°C.

The annealed samples lost the brown coloring and started to become white in color (Figure 4.4) with increasing annealing temperatures. At 900°C the sample remained white, however became non-translucent. A previous study by Srđić et al. in which zirconia nanocrystals were synthesized by chemical vapor synthesis also noted a brownish green color. According to Srđić, full density of the pressed ceramics is reached at around 950°C (Srđić et al., 2000). We assume that the origin of the samples losing translucency is enhanced light scattering and increase in pore size due to the enlargement of particle and cavity sizes when annealing at high temperatures (Laganovska et al., 2018; Smits et al., 2017). Several sets of samples were prepared and translucency achieved repeatedly. Annealing at various temperatures showed consistent results.



Figure 4.4: Pressed pellet (1 mm thickness) with no annealing (RT) and annealing at 500°C, 700°C, 800°C and 900°C temperatures (right).

Figure 4.5 shows XRD spectra of the  $\text{ZrO}_2$  powder as well as an unsintered pellet and pellets annealed at 750°C and 900°C. To ensure that the data is comparable the RT and 750°C spectra were taken of the same pellet before and after annealing. The data reveals an unexpected phase transformation from a mostly tetragonal phase powder sample to almost monoclinic phase when pressed in pellets (with monoclinic phase varying depending on annealing temperature from 68% to 84%, the rest being tetragonal phase) .

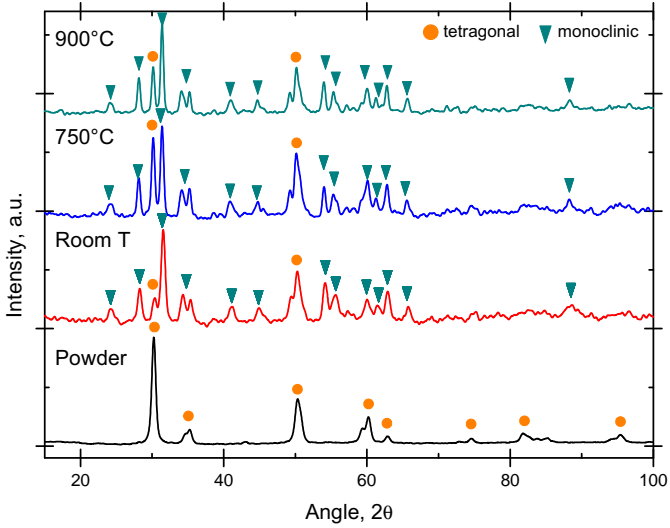


Figure 4.5: X-Ray diffraction data for the powder sample (black) and unsintered pellet (red), pellet annealed at 750°C (blue), and pellet annealed at 900°C (cyan).

To understand the phase transformation, stabilization processes in zirconia need to be considered. At ambient pressure  $\text{ZrO}_2$  has three polymorphs — monoclinic, tetragonal, and cubic. Only the monoclinic phase of the undoped  $\text{ZrO}_2$  is stable at room temperature (RT), however, the tetragonal and cubic phases can be stabilized by adding dopants with lower valence such as  $\text{Mg}^{2+}$ ,  $\text{Ca}^{2+}$ ,  $\text{Y}^{3+}$  (usually 3-14mol%) (Ćirić et al., 2020; Garvie, 1978; Kiisk et al., 2018). In our case, the  $\text{Er}^{3+}$  and  $\text{Yb}^{3+}$  concentration is too low and the tetragonal phase in powders is stabilized mainly by grain size (surface energy). Once the nanoparticles are pressed together, the surface energy reduces and the tetragonal phase is no longer able to remain stable and a phase transformation to monoclinic takes place. Srdić et al. observe a lower specific surface area for the pressed ceramics and explain it by the formation of contacts between individual particles decreasing the free surface area (Srdić et al., 2000). After ap-

plying a pressure of 250MPa, the ceramic acquires a brown color - a large amount of defects are created that stabilize the monoclinic phase, as the pressure is not high enough to start phase transformation to tetragonal - the transformation from monoclinic to tetragonal phase starts at around 2GPa Alzyab et al., 1987). By annealing at 750°C the defects disappear and tetragonal phase content slightly increases. By further annealing at 900°C rapid grain growth occurs, thus further reducing the surface impact in tetragonal phase stabilization. To understand the defect creation the samples were doped with Er for upconversion luminescence studies.

When comparing the up-conversion luminescence spectra between the pressed pellets and powder form, an increase in the red part of the spectrum relative to the green part can be seen (fig. ??). An overall decrease in the luminescence intensity can also be observed for the pressed sample. The red luminescence of the  $\text{Er}^{3+}$  ion is associated with cross-relaxation processes, which are correlated with the presence of defects near Er ions, therefore the position of  $\text{Er}^{3+}$  ions in the nanoparticles should be investigated further. Furthermore, the phase transformation from tetragonal in powders to monoclinic in ceramic pellets, could be the reason for the changes in upconversion luminescence.

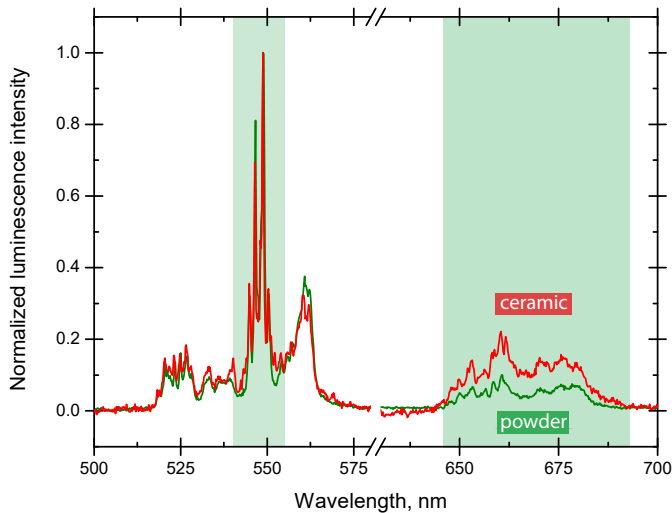


Figure 4.6: Up-conversion luminescence spectra for powder (green) and ceramic (red) samples before annealing.

When comparing the spectra of the annealed samples, it is shown in Figure 4.7 that the samples annealed at higher temperatures exhibit lower luminescence intensity in the red part of the spectrum relative to the green and have a higher total luminescence intensity. When annealed at  $900^{\circ}\text{C}$ , the luminescence intensity and red/green peak ratio returns to the level measured for powder sample, thus indicating that the crystalline phase affects upconversion luminescence less than intrinsic defect concentration. Until recently, it was believed that the decrease in photoluminescence that occurs at higher annealing temperatures is caused by the phase shift from tetragonal to monoclinic (Fabris et al., 2002; Garvie, 1978; Garvie, 1965; Torchynska et al., 2019). However, a study by Smits et al (Smits et al., 2017) showed that when a charge compensating element such as  $\text{Nb}^{5+}$  is incorporated into  $\text{ZrO}_2$  samples additionally to  $\text{Er}^{3+}$ , the phase change to monoclinic does not reduce photoluminescence intensity. Therefore the changes in the intensity of up-conversion luminescence can not be explained

by changes in the local crystal field that occur due to a phase shift and instead lanthanide ion positions and interaction with defects should be evaluated.

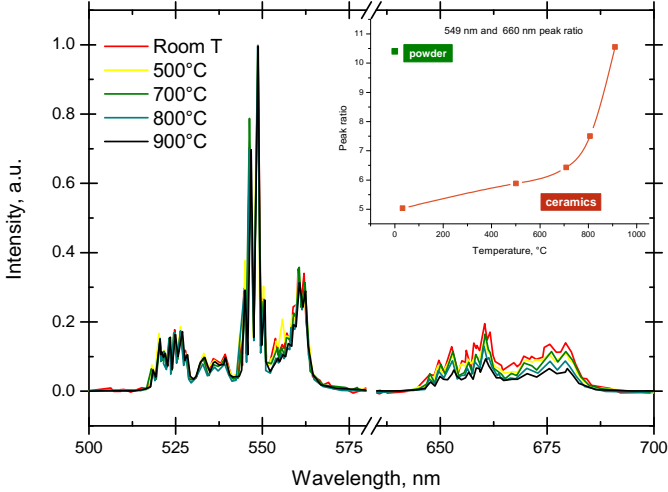


Figure 4.7: Up-conversion luminescence dependence on annealing temperatures.

It is known that cation (lanthanide) diffusion begins at around 1400°C, however anions start diffusing at 600°C (Smits et al., 2010). Therefore the changes in the luminescence spectra can be explained rather by intrinsic defects than by an increase in  $\text{Er}^{3+}$  cross-relaxation efficiency. If the increase in the red luminescence when pressing the samples into pellets was due to the distance between  $\text{Er}^{3+}$  ions becoming shorter, annealing would not have a large impact on the luminescence intensity. As a result of the annealing, oxygen vacancy diffusion and a decrease in defect amount takes place, which results in the increase of the total luminescence. Unlike pressed ceramics, the impact of heating up to 900°C has minimal impact on the luminescence intensity of the powder, which also indicates that the decrease of luminescence intensity after pressing and the subsequent in-

crease when pressed samples are annealed can be explained by intrinsic defects.

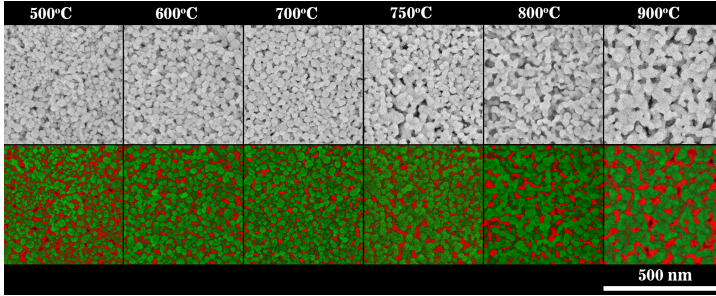


Figure 4.8: Top row: SEM images of pressed ceramic samples annealed at various temperatures. Bottom row: same images false colored to show particles (green) and pores (red).

Figure 4.8 shows SEM images of the pressed ceramics annealed at various temperatures. It can be seen that at low temperatures the pores (colored in red) are more abundant leading to less translucent samples. As the particle size increases with the annealing temperatures, the pores also change and become larger and fewer. During the sintering of zirconia nano-particles, small pores are eliminated and considerable growth of pores takes place. However at 900°C the particles (colored in green) have become too large and the sample becomes opaque. No shrinking was visible when the samples were annealed, meaning that the volume fraction of pores (i.e. the porosity) remains constant and only the pore size changes, becoming larger with higher annealing temperatures.

### 4.2.3 Conclusions

Translucent  $\text{ZrO}_2$  ceramics have been obtained by performing solar physical vapor deposition (SPVD) after sol-gel synthesis. The pressure of 250 MPa (diameter of pellet 5mm) is enough to create defects in nanocrystals of average size 25 nm. The luminescence quenching seen when pressing

the  $\text{ZrO}_2$  powder into pellets can be explained by the creation of intrinsic defects when pressure is applied rather than by the change in  $\text{Er}^{3+}$  ion cross-relaxation efficiency due to crystalline phase transformation. The annealing reduces the defects in ceramics thus increasing transparency, but at the same time, the pore size increases thus increasing light scattering.

#### 4.2.4 Thesis 2

The thesis of this study is therefore that erbium ion luminescence is an effective way of monitoring defect formation and phase transformation in nanostructured  $\text{ZrO}_2$  ceramics during the sintering process. When the samples were pressed into pellets, it was observed that the phase of the material is changed and intrinsic defects are created. Doping the materials with erbium, allowed studying this process in detail by analyzing the up-conversion luminescence data of the samples.

**Thesis 2: Erbium ion luminescence is an effective way of monitoring defect formation and phase transformation in nanostructured  $\text{ZrO}_2$  ceramics during the sintering process.**

## 4.3 Thermoluminescence study of oxygen vacancies in HfO<sub>2</sub>

### Hypothesis 3:

A hypothesis is put forward that Single (+1) and double (+2) charged oxygen vacancies at 3-fold coordinated ( $\text{VO}_3^{1+}$ ,  $\text{VO}_3^{2+}$ ) and 4-fold coordinated ( $\text{VO}_4^{1+} + \text{VO}_4^{2+}$ ) sites of monoclinic HfO<sub>2</sub> can be identified by thermoluminescence (TL). First, to obtain a large enough sample group for a reliable study, the samples are synthesized using various methods and materials that ensure that the defects present are not case-typical. These samples are then studied and correlations of different characteristics with the resulting thermoluminescence data are analyzed. Secondly, the samples are doped with europium to create oxygen vacancies in a controlled manner. This allows for direct observation of oxygen vacancy formation and behavior via changes in their thermoluminescence spectra.

### 4.3.1 Introduction

Thorough theoretical studies of intrinsic defects in undoped HfO<sub>2</sub> have been published (Chimata et al., 2019; Foster et al., 2002; Wang et al., 2016; Xiong and Robertson, 2005; Zheng et al., 2007) examining the probabilities of defect creation and stability under various conditions, however, complementary experimental studies have provided limited information (Aleksanyan et al., 2016; Gritsenko et al., 2016; Kiisk et al., 2010; Paperov et al., 2018; Perevalov et al., 2014).

The focus of this study therefore is on the oxygen vacancies found in hafnia studied using different methods of synthesis and thorough TL measurements, in addition with photoluminescence, XRD and TEM measurements. An in-depth analysis is enabled by combining two main factors: 1) various synthesis methods are used allowing to obtain more reliable and thorough data; 2) in addition to undoped HfO<sub>2</sub> samples were also doped

with  $\text{Eu}^{3+}$ . Rare-earth ions are often used as luminous probes of the local structure of the system in which they are embedded (Binnemans and Görrler-Walrand, 1996; Binnemans, 2015; Laganovska et al., 2018; Robert Hull, Jürgen Parisi, R. M. Osgood, Hans Warlimont, Guokui Liu, Bernard Jacquier, n.d.; Smits et al., 2017; Vitola et al., 2020), however in addition to that,  $\text{Eu}^{3+}$  ions are known to create oxygen vacancies when incorporated into  $\text{HfO}_2$  matrix. (Kiisk et al., 2010; Laganovska et al., 2018; Rajnak and Wybourne, 1964; Smits et al., 2017).

### 4.3.2 Results and discussion

Based on the need for the samples to have similar characteristics to ensure comparability and luminescent probes being affected more by the concentration of oxygen vacancies than the phase (Laganovska et al., 2018; Smits et al., 2017), the parameters of the synthesis methods were adjusted to achieve a monoclinic phase for all samples.

Samples from here on will be referred to as SG-PC (sol-gel polymerized complex), SG-G (sol-gel glycine), SG-U (sol-gel urea), CO-UH (combustion urea, HMTA), CO-U (combustion urea), CO-H (combustion HMTA), AIC (auto-ignition combustion), HYT (hydrothermal), PRE (precipitation).

Figure 4.10 shows TL glow peaks for undoped and 5 at% Eu doped samples after a 30 minute irradiation with X-rays. As samples are thought to largely emit photons in a similar mechanism to the photoluminescence process after the initial excitation via thermostimulation, the shown TL curves were corrected according to the PL intensities of the samples. Additionally, the TL curves were normalized with respect to the most intense TL peak (CO-UH undoped sample) in order to not lose information on the relative intensities of the peaks.

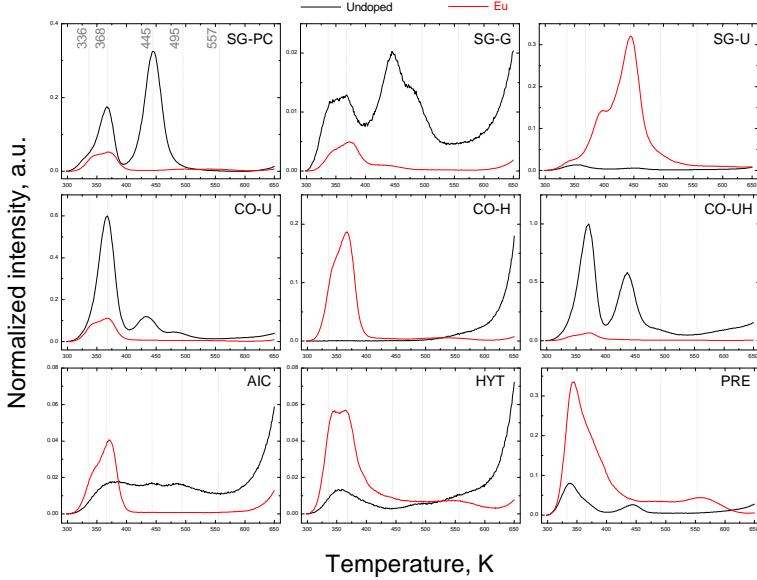


Figure 4.9: Thermoluminescence spectra for undoped  $\text{HfO}_2$  (black line) and 5 at% Eu doped (red line) samples with intensities normalized against the maximum value (undoped CO-UH).

The obtained trap activation energies using the equation 2.1 are shown in Table 4.1. It can be seen that largely there are five different traps located at energies:

- 1) 0.89 - 0.96 eV (336 K)
- 2) 1.00 - 1.08 eV (368 K)
- 3) 1.20 - 1.24 eV (445 K)
- 4) 1.35 - 1.40 eV (495 K)
- 5) 1.44 - 1.55 eV (557 K)

Theoretical studies provide valuable insights into trap activation energies of oxygen vacancies as well as defect formation energies. Although the seminal work of Foster et al. (Foster et al., 2002) had undervalued the

Table 4.1: Trap activation energies for undoped HfO<sub>2</sub> and Eu doped samples, eV

	Undoped				Eu			
SG-PC	0.89	1.00	1.23		0.95	1.02		1.54
SG-G	0.94	1.03	1.22	1.35	0.94	1.03	1.22	
SG-U	0.95	1.02	1.24		0.94	1.08	1.23	1.48
CO-U		1.01	1.24	1.35	0.96	1.00	1.20	1.44
CO-H					0.95	1.01		1.47
CO-UH		1.01	1.21	1.40	0.95	1.04	1.22	1.50
AIC		1.05	1.20	1.35	0.94	1.01		
HYT	0.94	1.01	1.11	1.38	0.95	1.04		1.50
PRE	0.92	1.02	1.23		0.95	1.06		1.55

band gap of HfO<sub>2</sub> (3.92 eV for the monoclinic phase), resulting in traps being located too close to valence band, when corrected for more recent theoretical values of the band gap (5.75 eV for the monoclinic phase), the values obtained are 1.10 eV for VO<sub>3</sub><sup>2+</sup> and 0.93 eV for VO<sub>3</sub><sup>1+</sup> and 1.43 eV for VO<sub>4</sub><sup>2+</sup> and 1.44 eV for VO<sub>4</sub><sup>1+</sup>. No electron affinity values for VO<sub>3</sub><sup>0</sup> and VO<sub>4</sub><sup>0</sup> were given by Foster.

Defect formation energies in undoped HfO<sub>2</sub> are provided by another seminal study by Zheng (Zheng et al., 2007) and Chimata (Chimata et al., 2019). While Chimata largely confirms the calculations of Zheng, only Zheng provides formation energies for VO<sub>3</sub> and VO<sub>4</sub> separately.

Zheng reports 1.12 eV, -1.66 eV, -4.83 eV and 0.98 eV, -1.39 eV, -4.20 eV for VO<sub>3</sub><sup>0</sup>, VO<sub>3</sub><sup>1+</sup>, VO<sub>3</sub><sup>2+</sup> and VO<sub>4</sub><sup>0</sup>, VO<sub>4</sub><sup>1+</sup>, VO<sub>4</sub><sup>2+</sup> under oxygen poor conditions respectively. A similar trend is seen under oxygen rich conditions, however the defect formation energies being higher with 0.81 eV and 1.44 eV for VO<sub>3</sub><sup>2+</sup> and VO<sub>4</sub><sup>2+</sup> respectively.

Based on these studies we propose the following assignment of defect types to the obtained TL curves:

**1) 0.89 - 0.96 eV (336K) - VO<sub>3</sub><sup>1+</sup>**

The theoretical trap depth is 0.93 eV (Foster et al., 2002). We obtained values in the range of 0.89 - 0.96 eV. Due to the "negative U" tendency of oxygen vacancies and VO<sub>3</sub><sup>1+</sup> not being stable against disproportionation

into  $\text{VO}_3^0$  and  $\text{VO}_3^{2+}$  (Chimata et al., 2019; Foster et al., 2002; Zheng et al., 2007), it is expected for there to be only a small amount of these defects found in undoped hafnia. This corresponds to the low 336 K TL peak intensity seen in the undoped samples and the increase of the peak intensity in Eu doped samples when the "negative U" tendency is disrupted.

**2) 1.00 - 1.08 eV (368K) -  $\text{VO}_3^{2+}$**

The theoretical trap depth is 1.10 eV (Foster et al., 2002). We obtained values in the range of 1.00 - 1.08 eV. Although the energy ranges do not correspond within the necessary range, we base this proposition on the observation that the the electron affinity for  $\text{VO}_3^{2+}$  is the most favorable and it is the most intense TL peak in the majority of the undoped samples as well as Eu doped samples.

**3) 1.20 - 1.24 eV (445K) -  $\text{VO}_4^{1+} + \text{VO}_4^{2+}$**

The theoretical trap depth is 1.44 and 1.43 eV for  $\text{VO}_4^{1+}$  and  $\text{VO}_4^{2+}$  correspondingly (Foster et al., 2002). We obtained values in the range of 1.20 - 1.24 eV. Here the difference between the theoretical values and the ones we have obtained is significant. However, based on the electron affinity being the second most favorable among  $\text{VO}_3$  and  $\text{VO}_4$  defects corresponding with the intensities of TL peaks and the already seen underestimation of trap depth with the previous defect type, the authors believe this to be the  $\text{VO}_4^{2+} + \text{VO}_4^{1+}$  defect peak. The difference between the theoretical values and our experimentally obtained ones might be explained by being due to Foster et al. using the theoretical band gap of 3.95 eV instead of 5.75 eV as has been calculated in more recent studies or a different frequency factor needing to be used for these traps (at  $s = 10^{-14}$  the obtained trap values are in the ranges 1.37-1.41 eV).

**4) 1.35 - 1.40 eV (495 K)**

Seen only in the undoped samples, it is possible that these might be oxygen interstitials  $\text{O}^0$  as Zheng (Zheng et al., 2007) provides point defect formation energies of 7.22 eV and 1.58 eV under oxygen-poor and rich

conditions respectively. Foster gives a corrected trap depth of 2.12 eV.

**5) 1.44 - 1.55 eV (557 K)** The peak overall is of very low intensity and found only in Eu doped samples. It is possible that this peak belongs to hafnium interstitials which appear when  $\text{Eu}^{3+}$  is introduced, however we do not speculate on this further.

### 4.3.3 Conclusions

For the first time a thorough experimental study of the possible intrinsic defects originating in hafnia has been performed. Trap depths for  $\text{VO}_3^{1+}$ ,  $\text{VO}_3^{2+}$ ,  $\text{VO}_4^{1+}$ ,  $\text{VO}_3^{2+}$  oxygen vacancies were evaluated from above room temperature TL data. Below room temperature TL measurements were also performed with further studies needed to determine the trap origin.

Additionally, when PL spectra were compared to TL wavelength spectra a potential indication of direct surface defect contribution to the resulting PL spectra was observed in both TL, XRL spectra and TEM images.

### 4.3.4 Thesis 3

Different types of oxygen vacancies in monoclinic  $\text{HfO}_2$  have been successfully identified by studying undoped and europium-doped samples and their thermoluminescence spectra. The experimentally identified vacancy characteristics strongly correlate with the theoretical calculations discussed in this study and section 2.1.1, confirming that identifying oxygen vacancies using thermoluminescence is a valid and reliable method.

**Thesis 3: Single (+1) and double (+2) charged oxygen vacancies at 3-fold coordinated ( $\text{VO}_3^{1+}$ ,  $\text{VO}_3^{2+}$ ) and 4-fold coordinated ( $\text{VO}_4^{1+} + \text{VO}_4^{2+}$ ) sites of monoclinic  $\text{HfO}_2$  can be identified by thermoluminescence.**

## 4.4 Europium ion incorporation characteristics in HfO<sub>2</sub>

### Hypothesis 4:

A hypothesis is formed that in monoclinic HfO<sub>2</sub>, Eu<sup>3+</sup> ions tend to incorporate in pairs as well as single ions, creating VO<sub>3</sub><sup>2+</sup> and VO<sub>3</sub><sup>1+</sup> oxygen vacancies. In order to prove this hypothesis, undoped and europium doped hafnia samples are synthesized and their characteristics analyzed. By using the information on the types of oxygen vacancies identified in thermoluminescence data acquired in the previous study, a further study on the properties of rare-earth ion incorporation into the host matrix is performed.

### 4.4.1 Introduction

Rare-earth ions are often used as luminescent probes to investigate the local structure of the system in which they are embedded, due to the well-defined electronic levels determined by their  $4f^n$  electronic configuration (Binnemans and Görrler-Walrand, 1996; Binnemans, 2015; Laganovska et al., 2018; Robert Hull, Jürgen Parisi, R. M. Osgood, Hans Warlimont, Guokui Liu, Bernard Jacquier, n.d.; Smits et al., 2017) and the shielding effect provided by the  $5s$  and  $5p$  electronic shells to the  $4f$  electrons (Rajnak and Wybourne, 1964). However the characteristics and effect of Eu<sup>3+</sup> ion incorporation into metal oxides from the experimental point of view have not been thoroughly investigated.

Therefore in this work we examine the properties of hafnia synthesized by various methods with an emphasis on the study of defects and the mechanisms of Eu<sup>3+</sup> incorporation into the host lattice. X-Ray diffraction, photoluminescence, luminescence decay kinetics and thermoluminescence measurements were performed in order to analyze the obtained samples.

## 4.4.2 Results and discussion

Although previous studies suggest that a more intense luminescence can be attained for tetragonal  $\text{HfO}_2$ , more recent studies have shown that the luminescence intensity is not as dependent on the phase of the material as it is on the distribution of oxygen vacancies (Laganovska et al., 2018; Smits et al., 2017). Based on this knowledge, the parameters of the synthesis methods were adjusted to achieve a monoclinic phase for all samples for the purpose of comparability.

Figure 4.10 shows TL glow peaks for undoped, 5 at% Eu doped and 5 at% Eu, 5 at% Nb doped samples after a 30 minute irradiation with X-rays. The TL curves were adjusted based on the PL intensities of the samples as it is believed that the photons are emitted in a mechanism similar to that seen in the photoluminescence process. To preserve information on the relative intensities of the peaks, the TL curves were additionally normalized in relation to the TL peak with the highest intensity (CO-UH undoped sample). It can be seen that as expected, when the samples are additionally doped with  $\text{Nb}^{5+}$ , the charge compensation reduces the amount of defects acting as traps as compared to undoped and  $\text{Eu}^{3+}$  doped samples. The Eu doped sample SG-U shows a significantly different behaviour from the rest of the samples. As this sample had used relatively larger amounts of urea during the synthesis, it is possible that some C or N impurities have remained in the final sample and this sample will not be taken into consideration in further analysis.

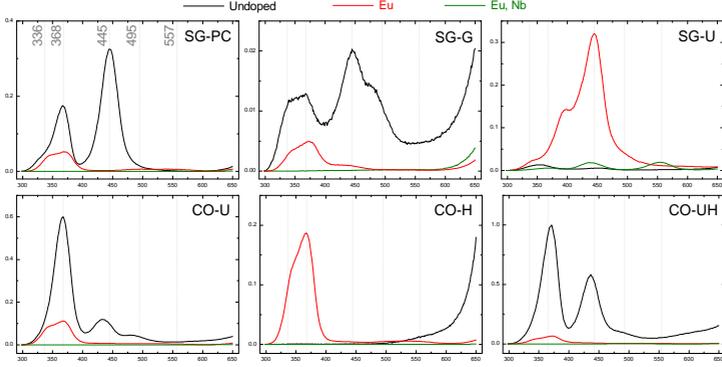


Figure 4.10: Thermoluminescence spectra for undoped  $\text{HfO}_2$  (black line), 5 at% Eu doped (red line) and 5 at% Eu, 5 at% Nb doped (green line) samples with intensities normalized against the maximum value (undoped CO-UH).

A previous publication by Laganovska et al. identified different defect types and energy ranges. The traps at 336K, 368K and 445K were identified as a threefold coordinated oxygen vacancy  $\text{VO}_3^{1+}$ , a threefold coordinated oxygen vacancy  $\text{VO}_3^{2+}$  and the fourfold coordinated oxygen vacancies  $\text{VO}_4^{1+}$  together with  $\text{VO}_4^{+3}$  respectively.

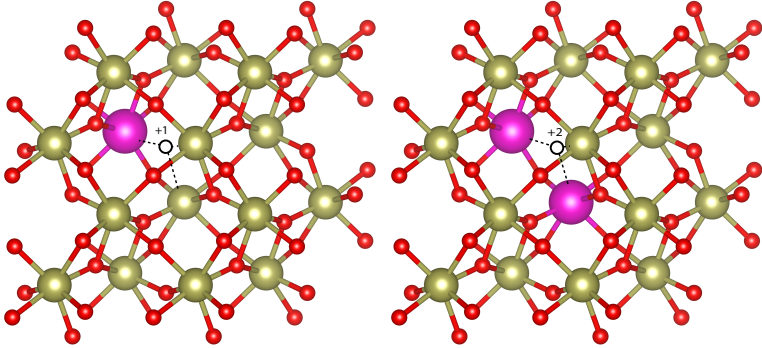


Figure 4.11: Possible incorporation of  $\text{Eu}^{3+}$  ions in the  $\text{HfO}_2$  matrix, (left) a  $\text{V}_\text{O}^+$  vacancy charge compensated by a single  $\text{Eu}^{3+}$ ; (right)  $\text{V}_\text{O}^{2+}$  charge compensated by two  $\text{Eu}^{3+}$  ions.

In this study, two novel aspects on the nature of  $\text{Eu}^{3+}$  ion incorporation into monoclinic  $\text{HfO}_2$  matrix is seen:

1) The  $\text{VO}_3^{1+}$  peak in undoped  $\text{HfO}_2$  has a very low TL intensity as is expected due to the "negative U" tendency (Foster et al., 2001) to disproportionate into  $\text{VO}_3^0$  and  $\text{VO}_3^{2+}$  vacancies. However, when doped with  $\text{Eu}^{3+}$ , the  $\text{VO}_3^{1+}$  peak at 336K greatly increases in intensity. This indicates that contrary to the previous proposal by Smits et al. (Smits et al., 2017) that  $\text{Eu}^{3+}$  ions mostly incorporate themselves in the host matrix in pairs so that the resulting oxygen vacancy charge  $\text{VO}_3^{2+}$  is compensated by two  $\text{Eu}^{3+}$  ions, a significant part of  $\text{Eu}^{3+}$  ions also incorporate themselves as single ions and create a stable  $\text{VO}_3^{1+}$  vacancy. An illustration is shown in Figure 4.11.

2) The  $\text{VO}_4^{1+}$  and  $\text{VO}_4^{2+}$  peak at 445K for most undoped samples is the second or even first highest glow peak. However, when doped with  $\text{Eu}^{3+}$  ions this peak disappears almost completely. The effect of threefold coordinated vacancy creation preference has been discussed in theoretical calculations, where Foster et al. (Foster et al., 2001) notes that the total system energy is much lower (0.44 eV and 0.76 eV, respectively) for the

threefold-coordinated site. This implies that although the formation of an initial neutral vacancy is energetically balanced between sites, once electrons are removed, the threefold coordinated oxygen vacancy is strongly favored for both  $\text{VO}_3^{1+}$  and  $\text{VO}_3^{2+}$ , and vacancies are likely to diffuse to these sites. It is therefore possible that when  $\text{Eu}^{3+}$  ions are incorporated into the matrix, the total system energy is lower when  $\text{Eu}^{3+}$  ions are located next to threefold coordinated oxygen vacancies and is thus the preferred site for  $\text{Eu}^{3+}$  ions as is seen in our experimental data.

### 4.4.3 Conclusions

$\text{HfO}_2$  doped with  $\text{Eu}^{3+}$  and  $\text{Eu}^{3+}$ ,  $\text{Nb}^{5+}$  of monoclinic structure and crystallite sizes ranging between 17.3 nm and 42.5 nm has been studied. When doped with Nb, an expected decrease in the amount of oxygen vacancies is seen.

The analysis of thermoluminescence data shows that a significant amount of  $\text{Eu}^{3+}$  ions are incorporated into the host matrix not only in pairs that balance out a  $\text{V}_\text{O}^{2+}$  vacancy, but also as single ions located next to a  $\text{V}_\text{O}^{1+}$  vacancy.

$\text{Eu}^{3+}$  ion incorporation into the host matrix creates a significantly larger amount of threefold coordinated oxygen vacancies than fourfold coordinated oxygen vacancies. This finding agrees with theoretical calculations where the threefold coordinated oxygen vacancy has a much lower total system energy when electrons are removed. Therefore when  $\text{Eu}^{3+}$  ions are introduced, mainly threefold coordinated oxygen vacancies are created.

### 4.4.4 Thesis 4:

By analyzing the thermoluminescence data of the undoped and europium-doped samples, it was seen that when  $\text{Eu}^{3+}$  is incorporated into the matrix, not only a  $\text{V}_\text{O}^{2+}$  vacancy is formed (signifying that the ions are incorporated

into pairs), but a  $V_O^{1+}$  vacancy is formed as well. The  $V_O^{1+}$  vacancy is therefore hypothesized to be charge balanced by single  $\text{Eu}^{3+}$  ions, leading to the conclusion, that europium also incorporates in single ions. Additionally, a strong preference for threefold-coordinated oxygen vacancy formation is seen, providing valuable insight into the mechanism of rare-earth ion incorporation into metal-oxide materials in general.

**Thesis 4: In monoclinic  $\text{HfO}_2$ ,  $\text{Eu}^{3+}$  ions tend to incorporate in pairs as well as single ions, creating  $\text{VO}_3^{2+}$  and  $\text{VO}_3^{1+}$  oxygen vacancies.**

## 5.SUMMARY

This work was focused on the study of defects in hafnia and zirconia and their influence on the various properties of these metal oxides, often using luminescent probes to gain additional insight into these materials.

An important drawback of introducing lanthanides into metal oxides are the oxygen vacancies created as a result of charge disbalance. To mitigate this issue, charge compensation in hafnia and zirconia was studied. It was shown to be a successful approach in reducing the amount of oxygen vacancies, which was observed through a decrease in thermoluminescence intensity and an increase in photoluminescence intensity. As a result, the quantum efficiency of these materials was significantly enhanced.

Even more important, while it was previously assumed that the phase of the host material largely determines the luminescence properties of the dopants, when charge-compensated, the luminescence intensity kept increasing even as the phase changed from tetragonal to monoclinic. This change suggested that the presence of oxygen vacancies is the primary cause of changes in luminescence intensity, rather than changes in the phase of the material and the resulting local crystal field.

This behaviour was shown to be true also with up-conversion luminescence. We observed luminescence quenching in ceramic samples when powders were pressed into pellets. By studying the differences in up-conversion luminescence spectra at different annealing temperatures, it was determined that the cause of the quenching could not be due to a change in lanthanide ion cross-relaxation efficiency as a result of phase change with applied pressure, but was yet again the impact of intrinsic defect creation.

Seeing as oxygen vacancies played a significant role in the resulting properties of metal oxides, it was necessary to carry out an in-depth research on the oxygen vacancies themselves. Through the use of thermolu-

minescence and the study of samples synthesized using various methods, threefold- and fourfold- coordinated, singly and doubly charged oxygen vacancies in hafnia were identified experimentally for the first time. These results enable an easier and more in-detail identification of oxygen vacancies in future studies.

Finally, although lanthanides are widely used as luminescent probes to carry out studies on the materials they are incorporated into, the nature of the incorporation of these ions had not been fully studied. Therefore, building on the knowledge gained while studying oxygen vacancies in hafnia, it was shown that the incorporation of lanthanide ions into the host matrix creates specifically threefold-coordinated oxygen vacancies which the ions then locate next to. It was also observed that lanthanide ions tend to incorporate into the matrix as both single ions and in pairs, which provides a key insight into the behavior of lanthanide ions in metal oxides.

## 6. THESES

**Thesis 1:** The luminescence intensity of rare-earth ions in  $\text{HfO}_2$  is determined more by the vicinity and distribution of nearby oxygen vacancies than by phase transition from monoclinic to tetragonal.

**Thesis 2:** Erbium ion luminescence is an effective way of monitoring defect formation and phase transformation in nanostructured  $\text{ZrO}_2$  ceramics during the sintering process.

**Thesis 3:** Single (+1) and double (+2) charged oxygen vacancies at 3-fold coordinated ( $\text{VO}_3^{1+}$ ,  $\text{VO}_3^{2+}$ ) and 4-fold coordinated ( $\text{VO}_4^{1+}$ ,  $\text{VO}_4^{2+}$ ) sites of monoclinic  $\text{HfO}_2$  can be identified by thermoluminescence.

**Thesis 4:** In monoclinic  $\text{HfO}_2$ ,  $\text{Eu}^{3+}$  ions tend to incorporate in pairs as well as single ions, creating  $\text{VO}_3^{2+}$  and  $\text{VO}_3^{1+}$  oxygen vacancies.

# 7. LIST OF CONFERENCES AND PUBLICATIONS

## 7.1 Authors publications reflecting the thesis

### Thesis 1:

1. Smits, K., Olsteins, D., Zolotarjovs, A., **Laganovska, K.**, Millers, D., Ignatans, R., Grabis, J. *Doped zirconia phase and luminescence dependence on the nature of charge compensation* (2017) Scientific Reports, 7, art. no. 44453.
2. **Laganovska, K.**, Bite, I., Zolotarjovs, A., Smits, K. *Niobium enhanced europium ion luminescence in hafnia nanocrystals* (2018) Journal of Luminescence, 203, pp. 358-363.

### Thesis 2:

3. **Laganovska, K.**, Olsteins, D., Smits, K., Bite, I., Bikse, L. *Formation of translucent nanostructured zirconia ceramics* (2021) Journal of the European Ceramic Society, 41 (13), pp. 6641-6648.

### Thesis 3:

4. **Laganovska, K.**, Bite, I., Zolotarjovs, A., Einbergs, E., Vitola, V., Dile, M., Smits, K. *Thermostimulated luminescence analysis of oxygen vacancies in HfO<sub>2</sub> nanoparticles* (2023) Materials Research Bulletin, 167, art. no. 112409,.

### Thesis 4:

1. Smits, K., Olsteins, D., Zolotarjovs, A., **Laganovska, K.**, Millers, D., Ignatans, R., Grabis, J. *Doped zirconia phase and luminescence*

*dependence on the nature of charge compensation* (2017) Scientific Reports, 7, art. no. 44453.

5. **Laganovska, K.**, I. Bite, A. Zolotarjovs, E. Einbergs, V. Vitola, and M. Dile. *Eu<sup>3+</sup> ion incorporation in hafnia* – under review in Materials Research Bulletin

## 7.2 Other publications

(total: 15 publications, h-index: 7)

- Bite, I., **Laganovska, K.**, Vanags, E., Vitola, V. *Synthesis and characterization of translucent hafnia ceramics* (2023) *Materialia*, 32, art. no. 101887, .
- Kuzmin, A., Pudza, I., Dile, M., **Laganovska, K.**, Zolotarjovs, A. *Examining the Effect of Cu and Mn Dopants on the Structure of Zinc Blende ZnS Nanopowders* (2023) *Materials*, 16 (17), art. no. 5825
- Dile, M., **Laganovska, K.**, Zolotarjovs, A., Bite, I., Vanags, E., Kuzmin, A., Pudza, I., Smits, K. *The effect of surfactants and precursors on the structure and properties of ZnS:Cu nanocrystalline particles*, (2023) *Nano-Structures and Nano-Objects*, 35, art. no. 101023,
- Kuzmin, A., Dile, M., **Laganovska, K.**, Zolotarjovs, A. *Microwave-assisted synthesis and characterization of undoped and manganese doped zinc sulfide nanoparticles* (2022) *Materials Chemistry and Physics*, 290, art. no. 126583, .
- Vitola, V., **Laganovska, K.**, Bite, I., Einbergs, E., Millers, D. *The role of boric acid in optical information storage properties in Eu doped BaSi<sub>2</sub>O<sub>5</sub>* (2022) *Journal of Luminescence*, 243, art. no. 118682, . Cited 1 time.
- **Laganovska, K.**, Olsteins, D., Smits, K., Bite, I., Bikse, L. *Formation of translucent nanostructured zirconia ceramics* (2021) *Journal of the European Ceramic Society*, 41 (13), pp. 6641-6648. Cited 2 times.
- Einbergs, E., Zolotarjovs, A., Bite, I., Cipa, J., Vitola, V., **Laganovska, K.**, Trinkler, L. *Re-Evaluation of Chromium Doped Alumina for Dosimetric Applications* (2021) *Latvian Journal of Physics and Technical Sciences*, 58 (1), pp. 15-22. Cited 1 time.
- Vitola, V., Bite, I., Millers, D., Zolotarjovs, A.,

- Laganovska, K.**, Smits, K., Spustaka, A. *The boron effect on low temperature luminescence of SrAl<sub>2</sub>O<sub>4</sub>:Eu, Dy* (2020) *Ceramics International*, 46 (16), pp. 26377-26381. Cited 9 times.
- Karitans, V., **Laganovska, K.**, Kundzins, K. *Phase retrieval of a Kolmogorov phase screen from very sparse data using four binary masks* (2020) *Applied Optics*, 59 (27), pp. 8362-8369.
  - **Laganovska, K.**, Zolotarjovs, A., Vázquez, M., Mc Donnell, K., Liepins, J., Ben-Yoav, H., Karitans, V., Smits, K. *Portable low-cost open-source wireless spectrophotometer for fast and reliable measurements* (2020) *HardwareX*, 7, art. no. e00108. Cited 29 times.
  - Einbergs, E., Zolotarjovs, A., Bite, I., **Laganovska, K.**, Auzins, K., Smits, K., Trinkler, L. *Usability of Cr-doped alumina in dosimetry* (2019) *Ceramics*, 2 (3), pp. 525-535. Cited 5 times.
  - Zolotarjovs, A., Smits, K., **Laganovska, K.**, Bite, I., Grigorjeva, L., Auzins, K., Millers, D., Skuja, L. *Thermostimulated luminescence of plasma electrolytic oxidation coatings on 6082 aluminium surface* (2019) *Radiation Measurements*, 124, pp. 29-34. Cited 6 times.
  - Auzins, K., Zolotarjovs, A., Bite, I., **Laganovska, K.**, Vitola, V., Smits, K., Millers, D. *Phosphorescent Coatings on Aluminum Using Sr<sub>0.95</sub>Eu<sub>0.02</sub>Dy<sub>0.03</sub>Al<sub>2</sub>O<sub>4</sub> Powder and Plasma Electrolytic Oxidation* (2019) *Coatings*, 9 (12), art. no. 865, . Cited 3 times.
  - Bite, I., Kriekē, G., Zolotarjovs, A., **Laganovska, K.**, Liepina, V., Smits, K., Auzins, K., Grigorjeva, L., Millers, D., Skuja, L. *Novel method of phosphorescent strontium aluminate coating preparation on aluminum* (2018) *Materials and Design*, 160, pp. 794-802. Cited 32 times.
  - Gavrilović, T., **Laganovska, K.**, Zolotarjovs, A., Smits, K., Jovanović, D.J., Dramićanin, M.D. *High resolution luminescence spectroscopy and thermoluminescence of different size LaPO<sub>4</sub>:Eu<sup>3+</sup> nanoparticles* (2018) *Optical Materials*, 82, pp. 39-46. Cited 3 times.

## 7.3 Conferences

- E-MRS 2023 Fall Laganovska K., Bite I., Zolotarjovs A., Smits K. "Thermostimulated luminescence analysis of oxygen vacancies in HfO<sub>2</sub> nanoparticles", Warsaw, Poland, 2023
- Advanced Materials and Technologies Laganovska K., Bite I., Smits K. "Study of Defects in Hafnia via Luminescent Properties", Palanga, Lithuania, 2020
- Luminescent Detectors and Transformers of Ionizing Radiation K.Laganovska, K.Smits, I.Bite, A.Zolotarjovs, "Defect reduction and europium ion luminescence enhancement in hafnia nanocrystals", Prague, Czechia, 2017
- Advanced Materials and Technologies K. Laganovska, E.Einbergs, I. Bite, K. Smits, "Terbium Ion Luminescence in Zirconia Single Crystals and Nanocrystals", Palanga, Lithuania, 2017
- Functional Materials and Nanotechnologies K.Laganovska, I.Bite, K.Smits., "Optical properties of HfO<sub>2</sub> and HfO<sub>2</sub> : Eu<sup>3+</sup> synthesized by various methods", Riga, Latvia, 2017
- University of Latvia, Institute of Solid State Physics, 34. scientific conference K.Laganovska, I.Bite, K.Smits, "Niobium enhanced europium ion luminescence in hafnia nanocrystals", Riga, Latvia, 2017

## 8. ACKNOWLEDGEMENTS

The author sincerely expresses her gratitude to the scientific supervisor Dr.Phys. Krišjānis Šmits as well as the head of the Optical materials laboratory Dr.Phys. Aleksejs Zolotarjovs. No less significant is the support (both scientific and emotional) the author received from colleagues MSc.Chem. Ivita Bite and Dr.Phys. Virginija Vitola.

The help of colleagues from other laboratories, as well as staff of the Institute of Solid State Physics, is also greatly appreciated.

Additionally, the author wants to thank the Faculty of Physics, Mathematics and Optometry of the University of Latvia for the constant support in studies and research through various programs, consultations, software licensing, and seminars.

This research was partly supported by the ERDF project No.1.1.1.1/21/A/055.

Institute of Solid State Physics, University of Latvia as the Center of Excellence has received funding from the European Union's Horizon 2020 Framework Programme H2020-WIDESPREAD-01-2016-2017-TeamingPhase2 under grant agreement No. 739508, project CAMART<sup>2</sup>



LATVIJAS UNIVERSITĀTES  
CIETVIELU FIZIKAS INSTITŪTS  
INSTITUTE OF SOLID STATE PHYSICS  
UNIVERSITY OF LATVIA

## 9. REFERENCES

- Aarik, J., Mändar, H., Kirm, M., & Pung, L. (2004). Optical characterization of HfO<sub>2</sub> thin films grown by atomic layer deposition. *Thin Solid Films*, *466*(1), 41–47. <https://doi.org/10.1016/j.tsf.2004.01.110>
- Aleksanyan, E., Kirm, M., Feldbach, E., & Harutyunyan, V. (2016). Identification of f<sup>+</sup> centers in hafnia and zirconia nanopowders. *Radiat. Meas.*, *90*, 84–89. <https://doi.org/10.1016/j.radmeas.2016.01.001>
- Alzyab, B., Perry, C. H., & Ingel, R. P. (1987). High-pressure phase transitions in zirconia and yttria-doped zirconia. *J. Am. Ceram. Soc.*, *70*(10), 760–765. <https://doi.org/10.1111/j.1151-2916.1987.tb04876.x>
- Binnemans, K., & Görrler-Walrand, C. (1996). Application of the eu<sup>3+</sup> ion for site symmetry determination [Cited By :177]. *Journal of Rare Earths*, *14*(3), 179–180.
- Binnemans, K. (2015). Interpretation of europium(III) spectra. *Coord. Chem. Rev.*, *295*, 1–45. <https://doi.org/10.1016/j.ccr.2015.02.015>
- Böscke, T. S., Müller, J., Bräuhaus, D., Schröder, U., & Böttger, U. (2011). Ferroelectricity in hafnium oxide thin films. *Appl. Phys. Lett.*, *99*(10), 102903. <https://doi.org/10.1063/1.3634052>
- Chau, R., Datta, S., Doczy, M., Doyle, B., Kavalieros, J., & Metz, M. (2004). High- $\kappa$ /metal-gate stack and its MOSFET characteristics. *IEEE Electron Device Lett.*, *25*(6), 408–410.
- Chen, R., & Winer, S. A. A. (1970). Effects of various heating rates on glow curves. *J. Appl. Phys.*, *41*(13), 5227–5232. <https://doi.org/10.1063/1.1658652>
- Chimata, R., Shin, H., Benali, A., & Heinonen, O. (2019). Defect energetics of cubic hafnia from quantum monte carlo simulations.

- Phys. Rev. Materials*, 3(7), 075005. <https://doi.org/10.1103/PhysRevMaterials.3.075005>
- Ćirić, A., Aleksić, J., Barudžija, T., Antić, Ž., Đorđević, V., Medić, M., Periša, J., Zeković, I., Mitrić, M., & Dramićanin, M. D. (2020). Comparison of three ratiometric temperature readings from the  $\text{Er}^{3+}$  upconversion emission. *Nanomaterials*, 10(4), 1–10. <https://doi.org/10.3390/nano10040627>
- Fabris, S., Paxton, A. T., & Finnis, M. W. (2002). A stabilization mechanism of zirconia based on oxygen vacancies only. *Acta Materialia*, 50(20), 5171–5178. [https://doi.org/10.1016/S1359-6454\(02\)00385-3](https://doi.org/10.1016/S1359-6454(02)00385-3)
- Foster, A. S., Lopez Gejo, F., Shluger, A. L., & Nieminen, R. M. (2002). Vacancy and interstitial defects in hafnia. *Phys. Rev. B Condens. Matter*, 65(17), 174117. <https://doi.org/10.1103/PhysRevB.65.174117>
- Foster, A. S., Sulimov, V. B., Lopez Gejo, F., Shluger, A. L., & Nieminen, R. M. (2001). Structure and electrical levels of point defects in monoclinic zirconia. *Phys. Rev. B Condens. Matter*, 64(22), 224108. <https://doi.org/10.1103/PhysRevB.64.224108>
- Franta, D., Ohlídal, I., Nečas, D., Vižd'a, F., Caha, O., Hasoň, M., & Pokorný, P. (2011). Optical characterization of  $\text{HfO}_2$  thin films. *Thin Solid Films*, 519(18), 6085–6091. <https://doi.org/10.1016/j.tsf.2011.03.128>
- Garvie, R. C. (1978). Stabilization of the tetragonal structure in zirconia microcrystals. *Journal of Physical Chemistry*, 82(2), 218–224. <https://doi.org/10.1021/j100491a016>
- Garvie, R. C. (1965). The Occurrence of Metastable Tetragonal Zirconia as a Crystallite Size Effect. *The Journal of Physical Chemistry*, 69(4), 1238–1243. <https://doi.org/10.1021/j100888a024>
- Gavartin, J. L., Muñoz Ramo, D., Shluger, A. L., Bersuker, G., & Lee, B. H. (2006). Negative oxygen vacancies in  $\text{HfO}_2$  as charge traps

- in high-k stacks. *Appl. Phys. Lett.*, *89*(8), 082908. <https://doi.org/10.1063/1.2236466>
- Gritsenko, V. A., Islamov, D. R., Perevalov, T. V., Aliev, V. S., Yelisseyev, A. P., Lomonova, E. E., Pustovarov, V. A., & Chin, A. (2016). Oxygen vacancy in hafnia as a blue luminescence center and a trap of charge carriers. *J. Phys. Chem. C Nanomater. Interfaces*, *120*(36), 19980–19986. <https://doi.org/10.1021/acs.jpcc.6b05457>
- Hu, J., Zhu, F., Matulionis, I., Deutsch, T., Gaillard, N., Miller, E., & Madan, A. (2009). Mater. Res. Soc. Symp. Proc. Vol. 1193 2009 Materials Research Society. *Materials Research*, *1193*(1), 2–7. <https://doi.org/10.1557/PROC-1144-LL16-04>
- Huang A.P., C. P. K., Yang Z.C. (2010). Hafnium-based high-k gate dielectrics. *Advances in Solid State Circuit Technologies*.
- Jiang, H., Gomez-Abal, R. I., Rinke, P., & Scheffler, M. (2010). Electronic band structure of zirconia and hafnia polymorphs from the *GW* perspective. *Phys. Rev. B Condens. Matter*, *81*(8), 085119.
- Kaichev, V. V., Ivanova, E. V., Zamoryanskaya, M. V., Smirnova, T. P., Yakovkina, L. V., & Gritsenko, V. A. (2013). XPS and cathodoluminescence studies of  $\text{HfO}_2$ ,  $\text{Sc}_2\text{O}_3$  and  $(\text{HfO}_2)_{1-x}(\text{Sc}_2\text{O}_3)_x$  films. *Eur. Phys. J. Appl. Phys.*, *64*(1), 10302. <https://doi.org/10.1051/epjap/2013130005>
- Kiisk, V., Lange, S., Utt, K., Tätte, T., Mändar, H., & Sildos, I. (2010). Photoluminescence of sol-gel-prepared hafnia. *Physica B Condens. Matter*, *405*(2), 758–762. <https://doi.org/10.1016/j.physb.2009.09.101>
- Kiisk, V., Puust, L., Mandar, H., Ritslaid, P., Rahn, M., Bite, I., Jankovica, D., Sildos, I., & Jaaniso, R. (2017). Phase stability and oxygen-sensitive photoluminescence of  $\text{ZrO}_2\text{:Eu,Nb}$  nanopowders. *Materials Chemistry and Physics*. <https://doi.org/10.1016/j.matchemphys.2018.04.090>
- Kiisk, V., Puust, L., Mändar, H., Ritslaid, P., Rahn, M., Bite, I., Jankovica, D., Sildos, I., & Jaaniso, R. (2018). Phase stability and oxygen-

- sensitive photoluminescence of  $\text{ZrO}_2\text{:Eu,Nb}$  nanopowders. *Mater. Chem. Phys.*, *214*, 135–142. <https://doi.org/10.1016/j.matchemphys.2018.04.090>
- Kirm, M., Aarik, J., Jürgens, M., & Sildos, I. (2005). Thin films of  $\text{HfO}_2$  and  $\text{ZrO}_2$  as potential scintillators. *Nucl. Instrum. Methods Phys. Res. A*, *537*(1), 251–255. <https://doi.org/10.1016/j.nima.2004.08.020>
- Kong, M., Li, B., Guo, C., Zeng, P., Wei, M., & He, W. (2019). The optical absorption and photoluminescence characteristics of evaporated and IAD  $\text{HfO}_2$  thin films. *Coat. World*, *9*(5), 307. <https://doi.org/10.3390/coatings9050307>
- Laganovska, K., Bite, I., Zolotarjovs, A., & Smits, K. (2018). Niobium enhanced europium ion luminescence in hafnia nanocrystals. *J. Lumin.*, *203*, 358–363. <https://doi.org/10.1016/j.jlumin.2018.06.069>
- Langford, J. I., & Wilson, A. J. C. (1978). Scherrer after sixty years: A survey and some new results in the determination of crystallite size. *Journal of Applied Crystallography*, *11*(2), 102–113. <https://doi.org/10.1107/S0021889878012844>
- Liu, L. X., Ma, Z. W., Xie, Y. Z., Su, Y. R., Zhao, H. T., Zhou, M., Zhou, J. Y., Li, J., & Xie, E. Q. (2010). Photoluminescence of rare earth<sup>3+</sup> doped uniaxially aligned  $\text{HfO}_2$  nanotubes prepared by sputtering with electrospun polyvinylpyrrolidone nanofibers as templates. *J. Appl. Phys.*, *107*(2), 024309. <https://doi.org/10.1063/1.3290974>
- Manikantan, J., Ramalingam, H. B., Shekar, B. C., Murugan, B., Kumar, R. R., & Santhoshi, J. S. (2017). Physical and optical properties of  $\text{HfO}_2$  NPs – synthesis and characterization in finding its feasibility in opto-electronic devices. *Adv. Powder Technol.*, *28*(7), 1636–1646. <https://doi.org/10.1016/j.apt.2017.03.022>
- McKeever, S. W. S. (1983, July). *Thermoluminescence of solids* McKeever. Cambridge University Press.

- Meng, J., Jiang, D. Y., & Li, Q. (2010). Luminescent properties of  $\text{Eu}^{3+}$ -doped  $\text{HfO}_2$  powders prepared by combustion. *Key Eng. Mater.*, *434-435*, 805–807.
- Moore, G. E. (1975). Progress in digital integrated electronics. *Electron Devices Meeting*.
- Muñoz Ramo, D., Gavartin, J. L., Shluger, A. L., & Bersuker, G. (2007). Spectroscopic properties of oxygen vacancies in monoclinic  $\text{HfO}_2$  calculated with periodic and embedded cluster density functional theory. *Phys. Rev. B Condens. Matter*, *75*(20), 205336. <https://doi.org/10.1103/PhysRevB.75.205336>
- Muñoz Ramo, D., Shluger, A. L., Gavartin, J. L., & Bersuker, G. (2007). Theoretical prediction of intrinsic self-trapping of electrons and holes in monoclinic  $\text{HfO}_2$ . *Phys. Rev. Lett.*, *99*(15), 155504. <https://doi.org/10.1103/PhysRevLett.99.155504>
- Papernov, S., Brunsman, M. D., Oliver, J. B., Hoffman, B. N., Kozlov, A. A., Demos, S. G., Shvydky, A., Cavalcante, F. H. M., Yang, L., Menoni, C. S., Roshanzadeh, B., Boyd, S. T. P., Emmert, L. A., & Rudolph, W. (2018). Optical properties of oxygen vacancies in  $\text{HfO}_2$  thin films studied by absorption and luminescence spectroscopy. *Opt. Express*, *26*(13), 17608–17623. <https://doi.org/10.1364/OE.26.017608>
- Patra, A., Friend, C. S., Kapoor, R., & Prasad, P. N. (2002). Upconversion in  $\text{Er}^{3+}:\text{ZrO}_2$  nanocrystals. *J. Phys. Chem. B*, *106*(8), 1909–1912. <https://doi.org/10.1021/jp013576z>
- Perevalov, T. V., Aliev, V. S., Gritsenko, V. A., Saraev, A. A., & Kaichev, V. V. (2013). Electronic structure of oxygen vacancies in hafnium oxide. *Microelectron. Eng.*, *109*, 21–23. <https://doi.org/10.1016/j.mee.2013.03.005>
- Perevalov, T. V., Aliev, V. S., Gritsenko, V. A., Saraev, A. A., Kaichev, V. V., Ivanova, E. V., & Zamoryanskaya, M. V. (2014). The origin of 2.7 eV luminescence and 5.2 eV excitation band in hafnium oxide.

- Appl. Phys. Lett.*, 104(7), 071904. <https://doi.org/10.1063/1.4865259>
- Petrik, N. G., Taylor, D. P., & Orlando, T. M. (1999). Laser-stimulated luminescence of yttria-stabilized cubic zirconia crystals. *J. Appl. Phys.*, 85(9), 6770–6776. <https://doi.org/10.1063/1.370192>
- Puust, L., Kiisk, V., Eltermann, M., Mändar, H., Saar, R., Lange, S., Sildos, I., Dolgov, L., Matisen, L., & Jaaniso, R. (2017). Effect of ambient oxygen on the photoluminescence of sol–gel-derived nanocrystalline  $\text{zrO}_2\text{:eu,nb}$ . *Journal of Physics D: Applied Physics*, 50(21), 215303.
- Rajnak, K., & Wybourne, B. G. (1964). Configuration interaction in crystal field theory. *J. Chem. Phys.*, 41(2), 565–569. <https://doi.org/10.1063/1.1725909>
- Robert Hull, Jürgen Parisi, R. M. Osgood, Hans Warlimont, Guokui Liu, Bernard Jacquier (Ed.). (n.d.). *Spectroscopic properties of rare earths in optical materials*. Springer Berlin Heidelberg. <https://doi.org/10.1007/3-540-28209-2>
- Robertson, J., Xiong, K., & Clark, S. J. (2006). Band gaps and defect levels in functional oxides. *Proceedings of the Fourth International Symposium on Transparent Oxide Thin Film for Electronics and Optics (TOEO-4)*, 496(1), 1–7. <https://doi.org/10.1016/j.tsf.2005.08.175>
- Rosenblatt, G. H., Rowe, M. W., Williams, G. P., Jr, Williams, R. T., & Chen, Y. (1989). Luminescence of F and f+ centers in magnesium oxide. *Phys. Rev. B Condens. Matter*, 39(14), 10309–10318. <https://doi.org/10.1103/physrevb.39.10309>
- Shilov, A. O., Savchenko, S. S., Vokhmintsev, A. S., Gritsenko, V. A., & Weinstein, I. A. (2022). Thermal quenching of self-trapped exciton luminescence in nanostructured hafnia. *J. Lumin.*, 247, 118908. <https://doi.org/10.1016/j.jlumin.2022.118908>
- Smits, K., Sarakovskis, A., Grigorjeva, L., Millers, D., & Grabis, J. (2014). The role of nb in intensity increase of er ion upconversion lu-

- minescence in zirconia. *J. Appl. Phys.*, *115*(21), 213520. <https://doi.org/10.1063/1.4882262>
- Smits, K., Grigorjeva, L., Millers, D., Sarakovskis, A., Opalinska, A., Fidelus, J. D., & Lojkowski, W. (2010). Europium doped zirconia luminescence. *Opt. Mater.*, *32*(8), 827–831. <https://doi.org/10.1016/j.optmat.2010.03.002>
- Smits, K., Jankovica, D., Sarakovskis, A., & Millers, D. (2013). Up-conversion luminescence dependence on structure in zirconia nanocrystals. *Opt. Mater.*, *35*(3), 462–466. <https://doi.org/10.1016/j.optmat.2012.09.038>
- Smits, K., Olsteins, D., Zolotarjovs, A., Laganovska, K., Millers, D., Ignatans, R., & Grabis, J. (2017). Doped zirconia phase and luminescence dependence on the nature of charge compensation. *Sci. Rep.*, *7*, 44453. <https://doi.org/10.1038/srep44453>
- Srdić, V., Winterer, M., & Hahn, H. (2000). Sintering behavior of nanocrystalline zirconia prepared by chemical vapor synthesis [cited By 111]. *Journal of the American Ceramic Society*, *83*(4), 729–736. <https://doi.org/10.1111/j.1151-2916.2000.tb01266.x>
- Tamrakar, R. K., Bisen, D. P., & Upadhyay, K. (2015). Photoluminescence behavior of  $\text{ZrO}_2$ :  $\text{Eu}^{3+}$  with variable concentration of  $\text{eu}^{3+}$  doped phosphor. *Journal of Radiation Research and Applied Sciences*, *8*(1), 11–16. <https://doi.org/10.1016/j.jrras.2014.10.004>
- Torchynska, T., El Filali, B., Khomenkova, L., Portier, X., & Gourbilleau, F. (2019). Phase transformation and light emission in Er-doped Si-rich  $\text{HfO}_2$  films prepared by magnetron sputtering. *Journal of Vacuum Science & Technology A*, *37*(3), 031503. <https://doi.org/10.1116/1.5085143>
- Villa, I., Lauria, A., Moretti, F., Fasoli, M., Dujardin, C., Niederberger, M., & Vedda, A. (2018). Radio-luminescence spectral features and fast emission in hafnium dioxide nanocrystals. *Phys. Chem. Chem. Phys.*, *20*(23), 15907–15915. <https://doi.org/10.1039/C8CP01230J>

- Villa, I., Vedda, A., Fasoli, M., Lorenzi, R., Kränzlin, N., Rechberger, F., Ilari, G., Primc, D., Hattendorf, B., Heiligtag, F. J., Niederberger, M., & Lauria, A. (2016). Size-Dependent luminescence in HfO<sub>2</sub> nanocrystals: Toward white emission from intrinsic surface defects. *Chem. Mater.*, *28*(10), 3245–3253. <https://doi.org/10.1021/acs.chemmater.5b03811>
- Vitola, V., Bite, I., Millers, D., Zolotarjovs, A., Laganovska, K., Smits, K., & Spustaka, A. (2020). The boron effect on low temperature luminescence of SrAl<sub>2</sub>O<sub>4</sub>:Eu, dy. *Ceram. Int.*, *46*(16, Part B), 26377–26381. <https://doi.org/10.1016/j.ceramint.2020.01.208>
- Wang, B., Wang, M., Duan, F., Ren, J., Li, Y., & Zhou, T. (2016). First principles study of defects in high-k hfo<sub>2</sub>. *Superlattices Microstruct.*, *99*, 88–93. <https://doi.org/10.1016/j.spmi.2016.05.001>
- Xiong, K., & Robertson, J. (2005). Point defects in HfO<sub>2</sub> high K gate oxide. *Microelectron. Eng.*, *80*, 408–411. <https://doi.org/10.1016/j.mee.2005.04.098>
- Yamashita, I., Kudo, M., & Tsukuma, K. (2012). Development of highly transparent zirconia ceramics. *Tosoh Res. Tech. Review*, *56*, 11–16.
- Zheng, J. X., Ceder, G., Maxisch, T., Chim, W. K., & Choi, W. K. (2007). First-principles study of native point defects in hafnia and zirconia. *Phys. Rev. B Condens. Matter*, *75*(10), 104112. <https://doi.org/10.1103/PhysRevB.75.104112>